Chemical Science

Accepted Manuscript

This article can be cited before page numbers have been issued, to do this please use: S. Amanullah and A. Dey, *Chem. Sci.*, 2020, DOI: 10.1039/D0SC01625J.

ROYAL SOCIETY OF CHEMISTRY

rsc.li/chemical-science

View Article Online
DOI: 10.1039/D0SC01625J

The Role of Porphyrin Peripheral Substituents in Determining the Reactivities of Ferrous Nitrosyl Species

Sk Amanullah, Abhishek Dey*

School of Chemical Sciences, Indian Association for the Cultivation of Science, 2A & 2B Raja SC Mullick Road, Kolkata, India – 700032

Supporting Information Placeholder

ABSTRACT: Ferrous nitrosyl $\{FeNO\}^7$ species are intermediates common to the catalytic cycles of Cd_1NiR and CcNiR, two heme-based nitrite reductases (NiR), and its reactivity vary dramatically in these enzymes. The former reduces NO_2^- to NO in the denitrification pathway while the latter reduces NO_2^- to NH_4^+ in dissimilatory nitrite reduction. With very similar electron transfer partners and heme based active sites, the origin of this difference in reactivity has remained unexplained. Differences in the structure of the heme *d₁* (Cd_1NiR), which bears electron-withdrawing groups and has saturated pyrroles, relative to heme *c* (CcNiR) is often invoked to explain these reactivities. A series of iron porphyrinoids, designed to model the electron-withdrawing peripheral substitution as well as the saturation present in heme *d₁* in Cd_1NiR, and their NO adducts were synthesized and their properties were investigated. The data clearly show that the presence of electron-withdrawing groups (EWGs) and saturated pyrroles together in a synthetic porphyrinoid (FeDEsC) weakens the Fe-NO bond in $\{FeNO\}^7$ adducts along with decreasing the bond dissociation free energies ($BDFE_{NH}$) of the $\{FeHNO\}^8$ species. The EWG raises the E° of $\{FeNO\}^{7/8}$ process, making the electron transfer (ET) facile, but decreases the pK_a of $\{FeNO\}^8$ species, making protonation (PT) difficult, while saturation has the opposite effect. The weakening of the Fe-NO bonding biases the $\{FeNO\}^7$ species of FeDEsC for NO dissociation, as in Cd_1NiR, which is otherwise set-up for a proton-coupled electron transfer (PCET) to form a $\{FeHNO\}^8$ species eventually leading to its further reduction to NH_4^+.

View Article Online
DOI: 10.1039/D0SC01625J

Introduction

Nitrite plays a vital role in the biochemical N-cycle.[1, 2] Being generated from nitrate by the action of a molybdenum-containing nitrate reductase[3], nitrite is consumed via several pathways which involve multiple heme and non-heme enzymes (Scheme 1A).[2] Assimilatory ammonification, catalyzed by siroheme containing nitrite reductase (CSNiR), and dissimilatory nitrite reduction, catalyzed by multi-*c* heme-containing nitrite reductase (CcNiR, Figure 1A), leads to the formation of ammonium ion (NH_4^+) directly, without releasing any intermediate nitrogenous species.[4] Alternatively, denitrification involves the reduction of nitrite to nitric oxide (NO), catalyzed by heme *cd*$_1$ containing nitrite reductase (Cd_1NiR, Figure 1B).[5] Further reduction of nitric oxide generates nitrous oxide,[6] which eventually reduced further to dinitrogen.[7, 8] Thus, CcNiR reduces nitrite to NH_4^+ without releasing any intermediate, and Cd_1NiR reduces nitrite to release NO. Both of these enzymes have heme cofactors in their active site with a very similar distal environment and electron transfer partners (Figure 1).

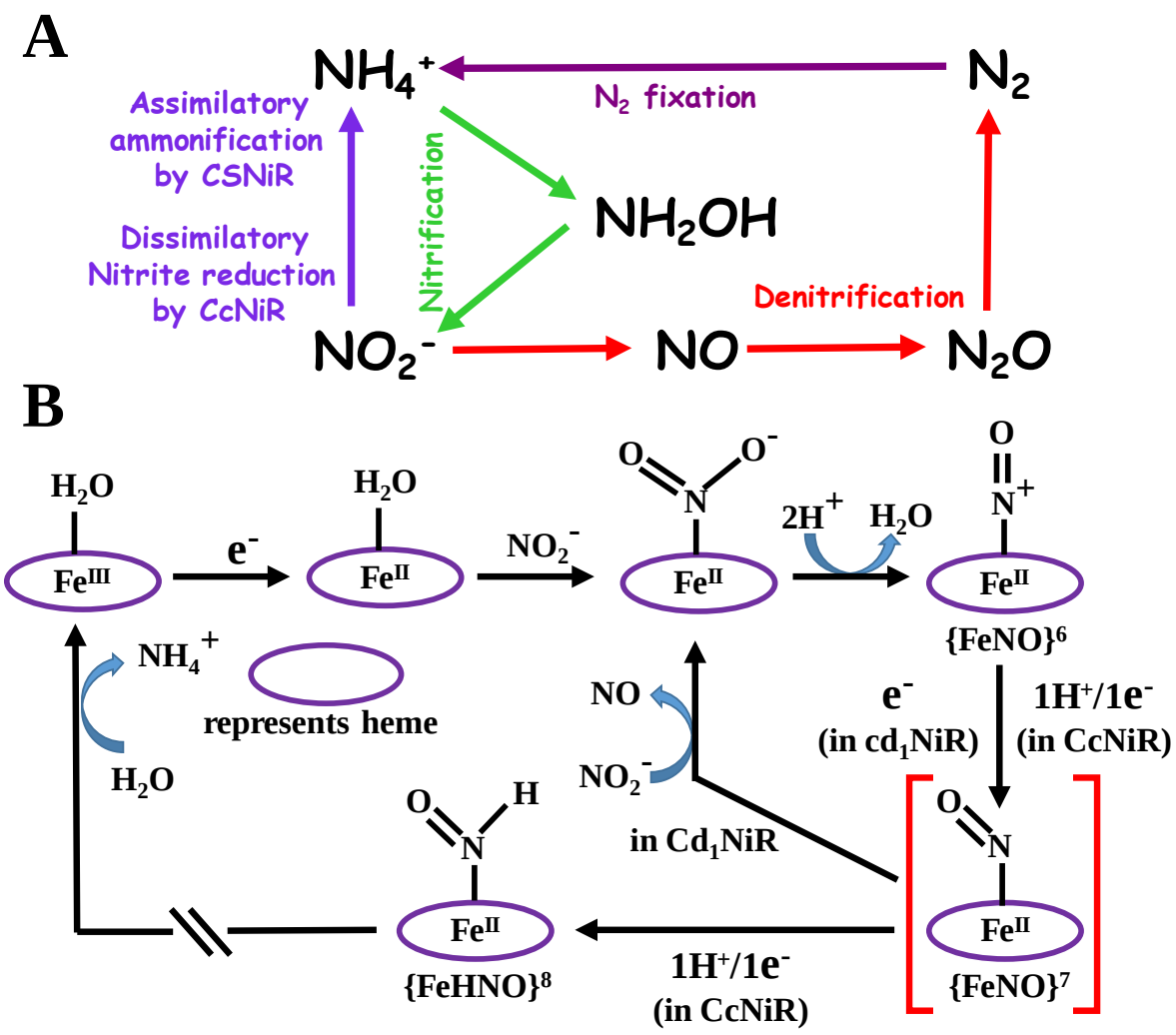

View Article Online
DOI: 10.1039/D0SC01625J

Scheme 1. (A) Selected components of the biochemical cycle of "N" and (B) Proposed mechanistic pathways of nitrite reduction catalyzed by CcNiR and Cd_1NiR.[2]

The proposed mechanistic pathways of both Cd_1NiR and CcNiR are quite similar (Scheme 1B).[2] The nitrite binds to the reduced ferrous iron center. With two protons from the distal residues, a molecule of water is released, forming a $\{FeNO\}^6$ intermediate (Enemark-Feltham notation).[5, 9, 10] The CcNiR avoids the formation of the dead-end intermediate, $\{FeNO\}^7$ through two consecutive proton-coupled electron transfer (PCET) to the $\{FeNO\}^6$ species, generating a $\{FeHNO\}^8$ intermediate,[11] which, on further reduction, leads to the generation of NH_4^+.[9] Alternatively, Cd_1NiR forms $\{FeNO\}^7$ through an electron transfer (ET) from cytochrome *c*, and releases NO with the concomitant binding of nitrite to the ferrous heme-d_1 and the cycle continues.[12-14] The different reactivity of $\{FeNO\}^7$ species compels investigating the difference in the active sites that control the competition between the PCET process and NO release. A $\{FeNO\}^7$ adduct generally possesses a very strong Fe-NO bond with a $K_d \sim 10^{-9}$ and this displacement of NO by nitrite is rather unexpected.[15] Although the N-O stretch of the $\{FeNO\}^7$ species of CcNiR is not reported, the N-O stretch of Cd_1NiR is higher than that of other known heme proteins like hemoglobin and myoglobin.[16-18] We find a strong positive correlation between the reported rate of NO dissociation and the corresponding N-O frequency (Figure 2A). It suggests that the rate of NO dissociation is reflected by the strength of Fe-NO bond, which is reflected in the N-O stretching vibration.[16-21] Similar correlation is also present between N-O stretching frequency and the rate of NO displacement by pyridine in different synthetic meso-phenyl substituted Fe-porphyrins (Figure 2B).[22] Iron-porphyrins bearing electron-withdrawing groups (EWGs), having higher N-O stretching frequency, release NO easier. Previous work from our group demonstrated that the iron-porphyrins bearing EWGs and/or saturated β-pyrrolic carbons form weaker iron-nitrosyls due to the competitive back-bonding between macrocycle π^* and NO π^*-orbitals from the filled Fe-d_π orbitals.[23]

View Article Online
DOI: 10.1039/D0SC01625J

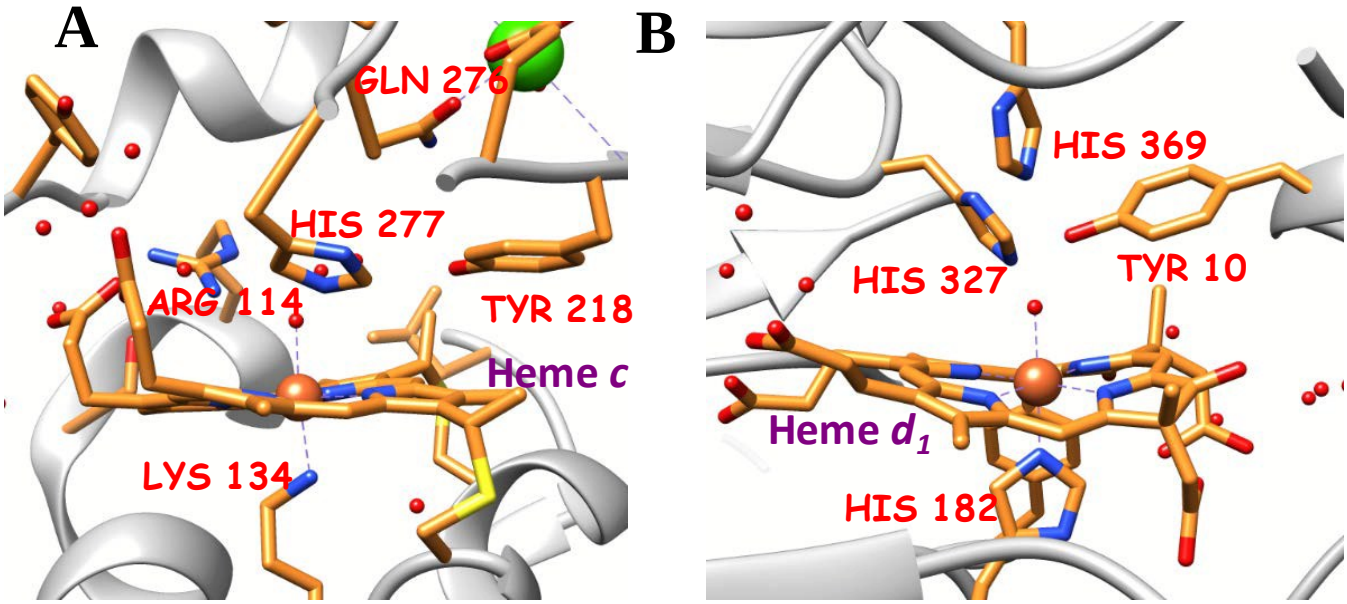

Figure 1. The active site structure of the nitrite reductases at resting state; A) CcNiR (pdb: 1FS7)[24] and B) Cd_1NiR (pdb: 1NIR)[25]; the figures are redrawn using software package Chimera 1.12rc.

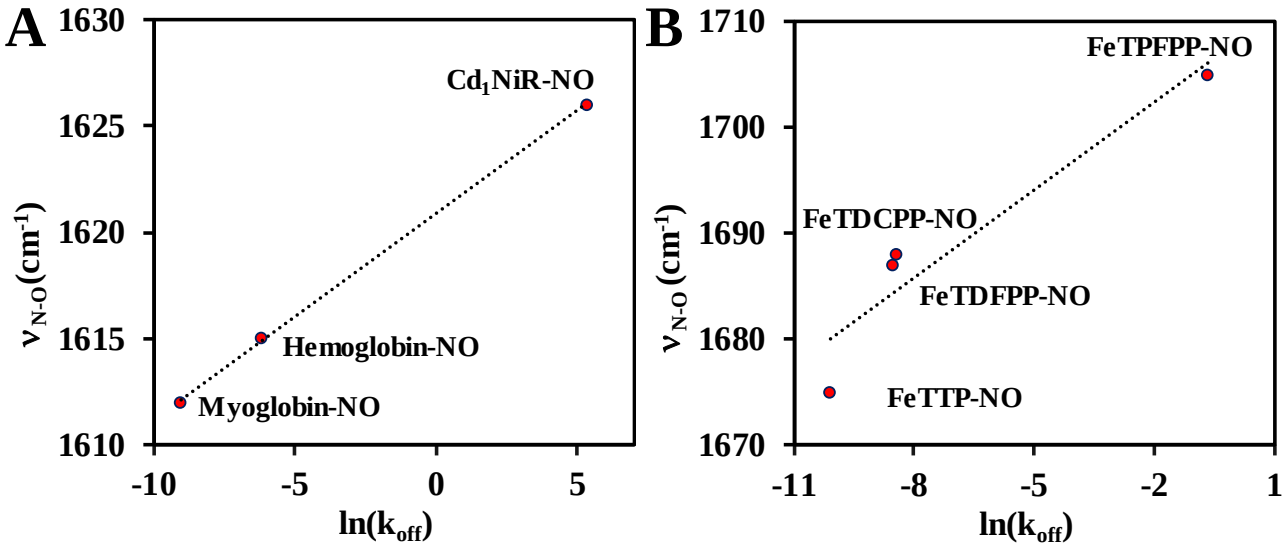

Figure 2. Correlation between N-O stretching frequency[16-18] and rate of NO dissociation[19-21]: A) in six-coordinate heme nitrosyls in enzyme systems; B) in synthetic Fe-porphyrin nitrosyl complexes, TTP (p-tolyl), TDFPP (2,6-difluorophenyl), TDCPP (2,6-dichlorophenyl), TPFPP (pentafluorophenyl).

CcNiR and Cd_1NiR possess basic 2nd sphere distal residues and primarily σ-donor Histidine or lysine axial ligands and same redox partner (cytochrome *c*). These residues assist in NO_2^- binding, proton translocation and is likely to affect the dissociation constants of NO_x ligands.[9, 11, 26, 27] Another major distinction is the difference in the nitrite binding sites: heme *c* in CcNiR, and heme d_1 in Cd_1NiR (Figure 1).[24, 25] The major difference in heme d_1, relative to heme *c* is the presence of two saturated β-pyrroles

View Article Online
DOI: 10.1039/D0SC01625J

(i.e., sp^3 hybridized peripheral carbons) along with two electron-withdrawing keto-groups (Figure 3).[28, 29] Therefore, their divergent reactivity may stem from differences in the structure of iron-porphyrinoid macrocycles. To evaluate this possibility, the electrochemistry of synthetic iron-porphyrin model complexes (FeTPP, FeOEP, FeOEPone and Fe(2,4-OEPdione), Figure 3) and their nitrosyl adducts have been investigated by several groups.[30-39] Under the coulometric condition, nitrite could be reduced to ammonium ion by the synthetic complexes mediated by a hydroxylamine bound species.[40-43] The rate of the reaction was strongly directed by the macrocycle i.e., FeOEP reacted faster than FeTPP and the reaction was very slow in the Fe(2,4-OEPdione) complex. The basicity of {FeNO}^{8} species could potentially explain the difference in reactivity.[42] Alternatively, the greater Lewis acidity of {Fe(2,4-OEPdione)-NO}^{7} (as suggested by facile pyridine binding to the Fe) was suggested to enhance the His-coordination with heme d_1 which might help the release of the trans NO.[33] These results herald the intrinsic nature of the macrocycle as a determinant of the different reactivity of the {FeNO}^{7} species i.e., NO release vs PCET. A {FeHNO}^{8} species (proceed after PCET to {FeNO}^{7}) is quite reactive and so far could only be transiently observed in protected environments such as proteins,[44, 45] or in bis-picket fence porphyrin[46] or in highly electron-rich FeOEP in the presence of weak acid such as substituted phenols.[41] Alternately, under electrochemical conditions, {FeNO}^{8} yields the parent {FeNO}^{7} species and H_2 .[43] It is important to understand the role of these peripheral modifications in the electronic structure and reactivity of these iron nitrosyls, to understand the different reactivities of the {FeNO}^{7} species exhibited by these enzymes.

View Article Online
DOI: 10.1039/D0SC01625J

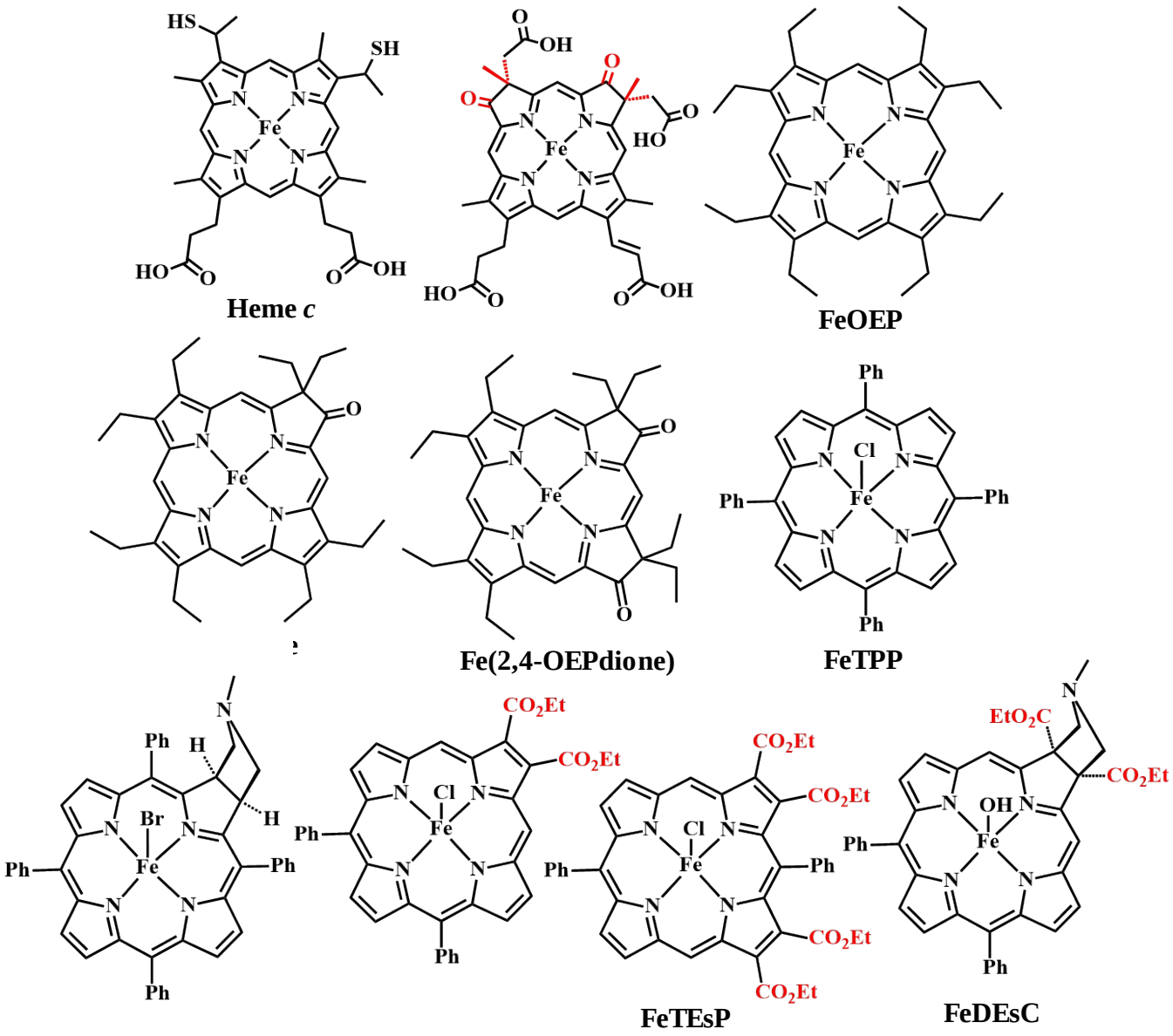

Figure 3. Structure of the naturally occurring heme and synthetic Fe-porphyrinoids. FeOEP, FeOEPone, and Fe(2,4-OEPdione) were synthesized previously.[32, 47, 48]

In this manuscript, a series of synthetic iron-porphyrins were developed for systematically varying in their peripheral substituents. By introducing EWGs and/or saturation at the β-pyrrolic positions, we were able to decode the role of each substituent on the basic iron-porphyrin skeleton on the electronic structure and reactivity of their corresponding $\{FeNO\}^7$ species. The electrochemical and spectroscopic data of their NO adducts and density functional theory (DFT) calculations help alienate the contribution of reduction potential and pK_a to the bond dissociation free energy ($BDFE_{NH}$) of the N-H bond in $\{FeHNO\}^8$ species. The results indicate a definitive role of EWG and saturation in tuning the Fe-NO bond strength, the

View Article Online
DOI: 10.1039/D0SC01625J

reduction potential of $\{FeNO\}^7$ and pK_a of $\{FeNO\}^8$ species, which can likely explain the origin of differences in the reactivity of CcNiR and Cd_1NiR.

Results

1. Synthesis

The heme involved in nitrite binding sites of CcNiR and Cd_1NiR is heme *c* and heme d_1, respectively. The major difference between these being the presence of two electron-withdrawing-keto groups and two saturated β-pyrrolic carbons in heme d_1 (Figure 3). To rationalize the effect of EWG and/or saturation, a series of iron-porphyrinoids were synthesized (Figure 3), namely, iron-tetraphenylporphyrin (FeTPP, fully unsaturated); iron-diesterporphyrin (FeDEsP, having two electron-withdrawing ester groups); iron-tetraesterporphyrin (FeTEsP, having four ester groups); iron-tetraphenylchlorin (FeTPC, having two saturated β-pyrrolic carbons) and iron-diesterchlorin (FeDEsC, having two ester groups and two saturated β-pyrrolic carbons). Those EWGs were designed to qualitatively emulate the –I (inductive) effect of the keto-groups in heme d_1. FeTPP, FeTPC, FeDEsP, and FeDEsC complexes were synthesized following previously reported procedures.[23, 49]

View Article Online
DOI: 10.1039/D0SC01625J

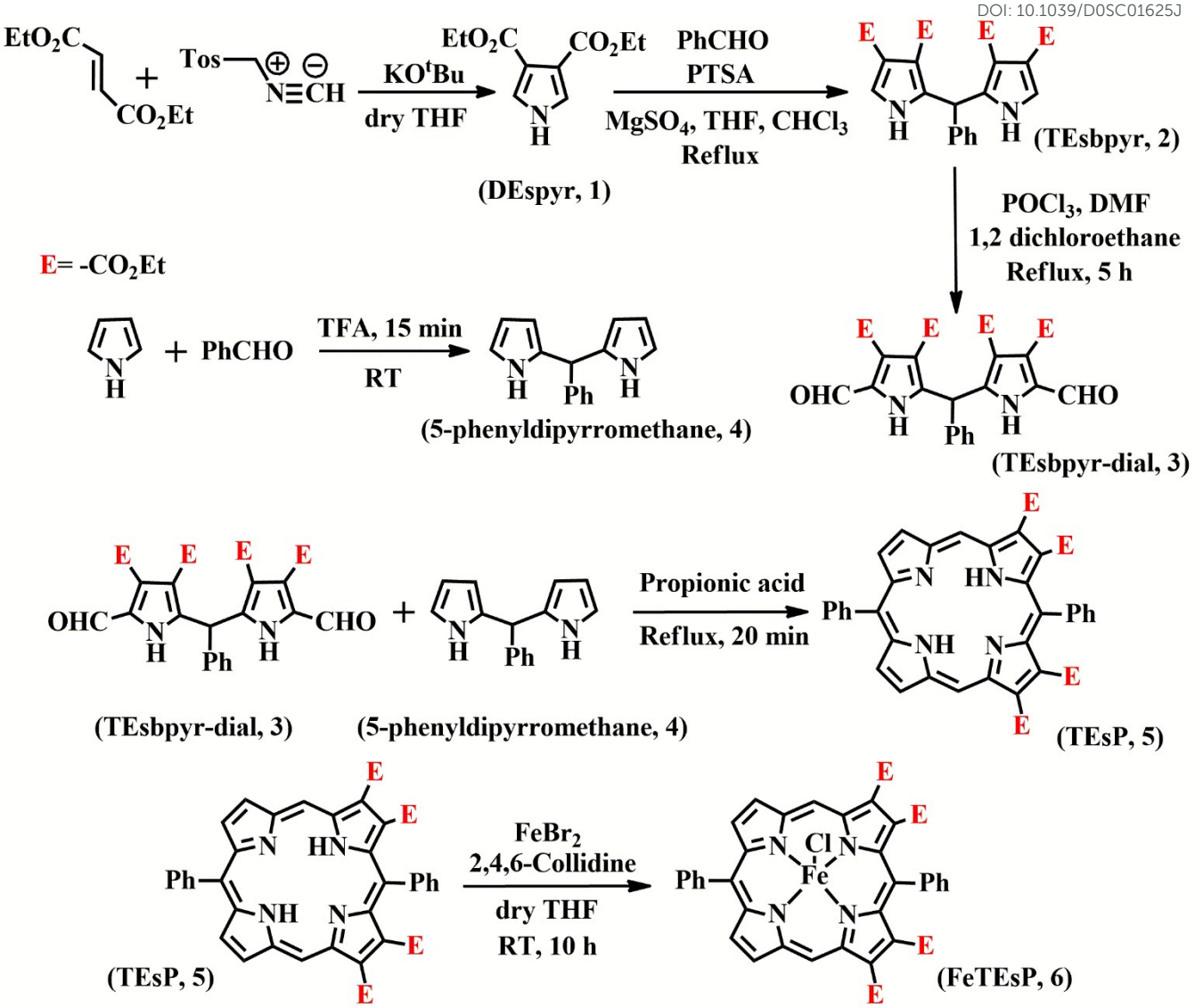

Scheme 2: Synthetic strategy of FeTEsP. In some cases, the –CO_2Et group is abbreviated as "E" for clarity in representation,

FeTEsP was synthesized to introduce four electron-withdrawing substitutions on the porphyrin ring. TEsP (5 in Scheme 2) was synthesized from the propionic acid condensation of two dipyrromethanes (Scheme 2). One of which (TEsbpyr-dial, 3 in Scheme 2) contained four ester groups (at the 3 and 4 positions of the respective pyrroles) as well as two aldehyde groups (at the 2 positions of the respective pyrroles) and the other half was 5-phenyldipyrromethane (4 in Scheme 2). Base induced cyclization of diethyl fumarate and *p*-toluenesulfonylmethylisocyanide (TosMIC) lead to the formation of pyrrole bearing two ester groups (DEspyr, 1 in Scheme 2). Dipyrromethane of DEspyr (TEsbpyr, 2 in Scheme 2) was obtained with the condensation with benzaldehyde under harsh acidic conditions. A Vilsmeier-Haack reaction was performed upon TEsbpyr to obtain the corresponding dialdehyde, TEsbpyr-dial (3 in Scheme 2).

View Article Online
DOI: 10.1039/D0SC01625J

The other half, i.e., the 5-phenyldipyrromethane (4 in Scheme 2), was prepared from acid-catalyzed condensation of pyrrole and benzaldehyde following the Lindsey protocol.[50] Zinc and iron metalation was performed using established protocols.[49] The zinc complex of TEsP was characterized by single-crystal XRD. Needle-shaped purple crystals of ZnTEsP were grown from the diffusion of hexane into a DCM solution of the complex (Figure 4C). It crystallized in a triclinic symmetry with a centrosymmetric P_{-1} space group. Structural analysis revealed that it was a dimer, formed by the coordination of a free carbonyl "oxygen" atom with the zinc atom of another molecule. The structures of FeDEsP and ZnDEsC were reported before and shown here for comparison (Figure 4A-B). Further investigations were performed with the nitrosyl adducts of the iron-bound porphyrinoids.

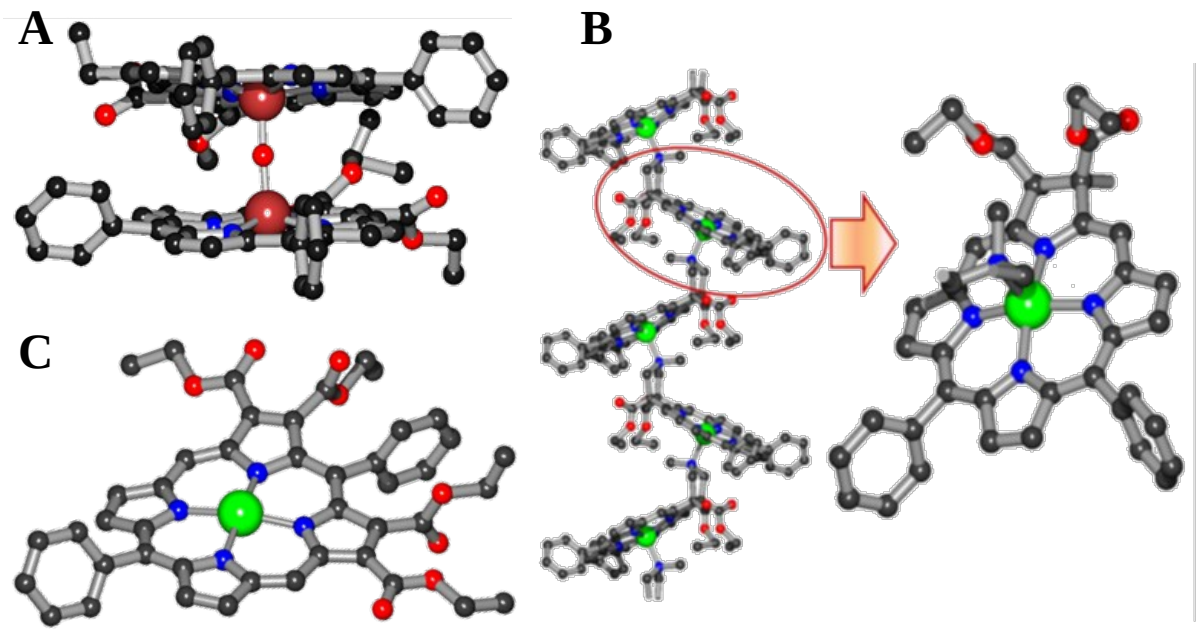

Figure 4: Molecular structure of the crystals of A) a μ-oxo dimer of FeDEsP; B) ZnDEsC, and C) ZnTEsP. Color code: C, black; Fe, brownish-red; Zn, green; N, blue; O, red. Hydrogen atoms are omitted for clarity.

2. Iron-nitrosyl reduction potentials

The cyclic voltammograms of the nitrosyl complexes of FeTPP, FeDEsP, FeTEsP, FeTPC, and FeDEsC showed an oxidation process at 0.20, 0.34, 0.38, -0.04 and 0.10 V, respectively, against Fc^{+}/Fc redox couple (Figure 5). For FeTPC and FeDEsC, the process was clearly observed only under fast scan rates (Figure S23B). The process was irreversible at slow scan rates, indicating dissociation of the NO during oxidation. Note that the CV of FeDEsC was performed under NO saturated condition to prevent NO loss from the complex. Past research from Ryan and Kadish group established the nature of these redox events: the oxidation wave of porphyrin $\{FeNO\}^{7}$ leads to the formation of Fe^{III}-NO species, while in the case of chlorins, bacterio/iso-bacteriochlorins,

View Article Online
DOI: 10.1039/D0SC01625J

and porphinone/porphinediones, the oxidation leads to the formation of Fe^{II}-NO species with the macrocycle-cation radical.[32, 33, 36, 51] The $\{FeNO\}^{7/8}$ process was observed for FeTPP, FeDEsP, FeTEsP, FeTPC, and FeDEsC at -1.41, -1.24, -1.14, -1.51 and -1.42 V, respectively, vs Fc^{+}/Fc redox couple (Figure 5). The values obtained for FeTPP were consistent with previous reports.[38] The pre-wave observed in the case of FeTPP (-1.32 V), FeDEsP (-1.17 V) and FeTPC (-1.38 V), might be due to ligand association, which disappeared at higher scan rates (Figure S23A) as reported by Kadish group earlier.[38, 52] In the case of FeDEsC, the irreversible pre-wave at ~ -1.22 V vs Fc^{+}/Fc redox couple was likely due to the direct electrochemical NO reduction[53] (NO saturated solution), as observed by the Kadish group during the reduction of Fe^{II}-TPP-NO and Fe^{II}-OEP-NO, in the presence of excess NO gas in the medium.[38]

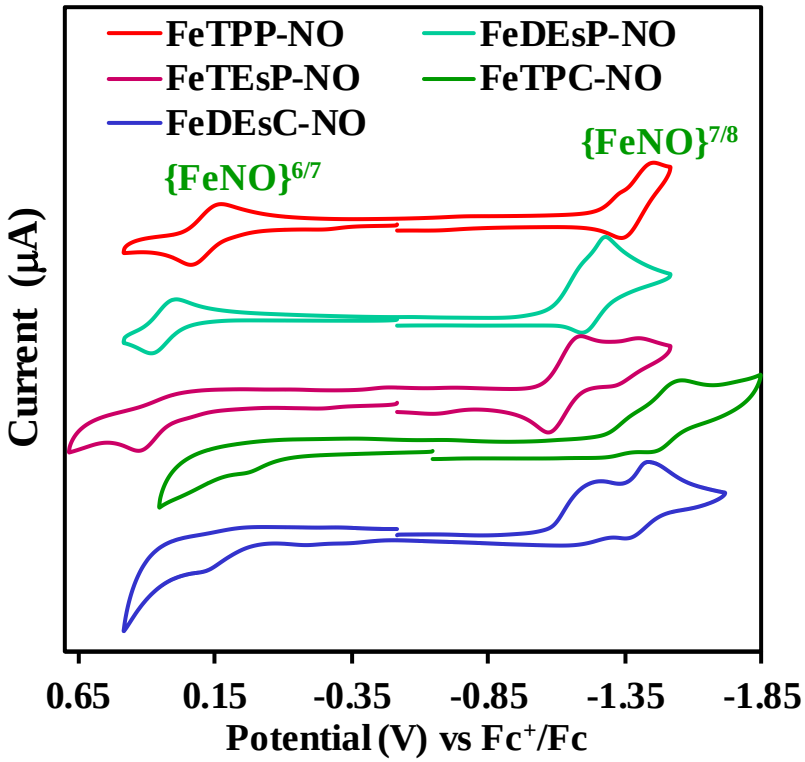

Figure 5: Cyclic voltammogram of the complexes in dichloromethane at room temperature. Working electrode: glassy carbon; counter electrode: platinum; reference electrode: aqueous Ag/AgCl in 4M KCl; Supporting electrolyte: tetrabutylammonium hexafluorophosphate (100 mM); scan rate: 50 mVps.

View Article Online
DOI: 10.1039/D0SC01625J

A clear trend was observed in both the oxidation and reduction process of the $\{FeNO\}^7$ species for the series of iron porphyrinoids used here. With an increase in the number of EWGs attached to the β-pyrroles relative to FeTPP-NO, both $\{FeNO\}^{6/7}$ and $\{FeNO\}^{7/8}$ couples shifted to higher potential (i.e., for FeDEsP-NO and FeTEsP-NO in Figure 5). Alternatively, saturating one of the pyrroles of FeTPP-NO, i.e., in the case of FeTPC-NO, both the reduction couples shifted to lower potentials. The FeDEsC-NO complex, having both EWGs as well as saturated pyrrole centers, had both the reduction potentials almost similar to those of FeTPP-NO. This implied that the EWG and saturation had opposite effects on the electronic structure of the Fe-NO unit.

3. Fe-NO bond strength

The FTIR data of the five-coordinate $\{FeNO\}^7$ complexes of FeTPP, FeDEsP, FeTEsP, FeTPC, and FeDEsC showed the N-O stretch at 1676, 1686, 1688, 1680 and 1691 cm^{-1}, respectively (Figure 6). The data showed that when two EWGs were introduced (FeDEsP), the N-O vibration (str.) shifted to 1686 cm^{-1} from 1676 cm^{-1} in FeTPP. Further addition of EWGs (FeTEsP), shifted the N-O vibration (str.) up to 1688 cm^{-1}. Such high N-O stretching frequencies had only been reported for $\{FeNO\}^7$ species of octa-halogenated porphyrins and reflect poor back-bonding between the occupied iron and unoccupied NO π^*-orbitals.[22, 54] The saturation of the pyrrole, by itself, exerted little effect on Fe-NO bonding as indicated by the N-O stretching frequency of $\{FeTPC\text{-}NO\}^7$ at 1680 cm^{-1} which was very similar to that of $\{FeTPP\text{-}NO\}^7$. But saturation along with EWGs caused a substantial weakening of the NO adduct, as indicated by the N-O stretch of $\{FeDEsC\text{-}NO\}^7$ at 1691 cm^{-1}, relative to $\{FeTPP\text{-}NO\}^7$ at 1676 cm^{-1}. The Fe-N stretch of the $\{FeNO\}^7$ species of FeTPP-NO reproduced previously reported value. However, despite several attempts with resonance Raman the Fe-N stretching frequencies could not be obtained for the other compounds studied (Figure S24A).[43] The strength of Fe-NO bond in the $\{FeNO\}^7$ adducts was strongly dictated by both σ-bonding and π-back-bonding.[55-58] As reported recently, the presence of electron-withdrawing substitutions on the porphyrin lowers the energy of the porphyrin π^*-orbitals. This results in competitive back-bonding from the filled d_π orbitals of Fe between porphyrin π^* and NO π^*-orbitals, which eventually weakens the NO adducts.[23] Saturation by itself had a minor effect on the back-bonding. However, saturation along with two EWGs had an enhanced effect on the weakening of the NO-adduct.

Qualitatively, similar trend was observed for N-methylimidazole bound six-coordinate $\{FeNO\}^7$ species where the N-O stretching vibrations for FeTPP, FeDEsP, FeTEsP, FeTPC, and FeDEsC were observed at 1626 cm^{-1}, 1641 cm^{-1}, 1646 cm^{-1}, 1635 $cm^{-1}$and 1633 cm^{-1}, respectively (Figure S25A). Therefore, axial primarily σ donor nitrogeneous ligand has a very limited effect on the electronic structure of these $\{FeNO\}^7$ complexes. Note that the N-O stretch of the $\{FeNO\}^7$ species in Cd_1NiR was 1626 cm^{-1} with heme d_1, relative to 1612 cm^{-1} in myoglobin with heme *b* (which neither have EWG nor saturation).[16-18]

View Article Online
DOI: 10.1039/D0SC01625J

The higher N-O stretching frequency in the Cd_1NiR (by 14 cm^{-1}) was indicative of a weaker Fe-NO bonding. And it was associated with a ~10^6 fold enhancement in NO dissociation rate from the $\{FeNO\}^7$ intermediate (Figure 2).[13, 19-21, 59] The 15 cm^{-1} upshifting of the N-O vibration observed here between FeDEsC and FeTPP mirrored the 14 cm^{-1} shift observed between Cd_1NiR and myoglobin suggesting a weakening of the Fe-NO bond, raising the possibility of ligands like NO_2^- displacing the bound NO.

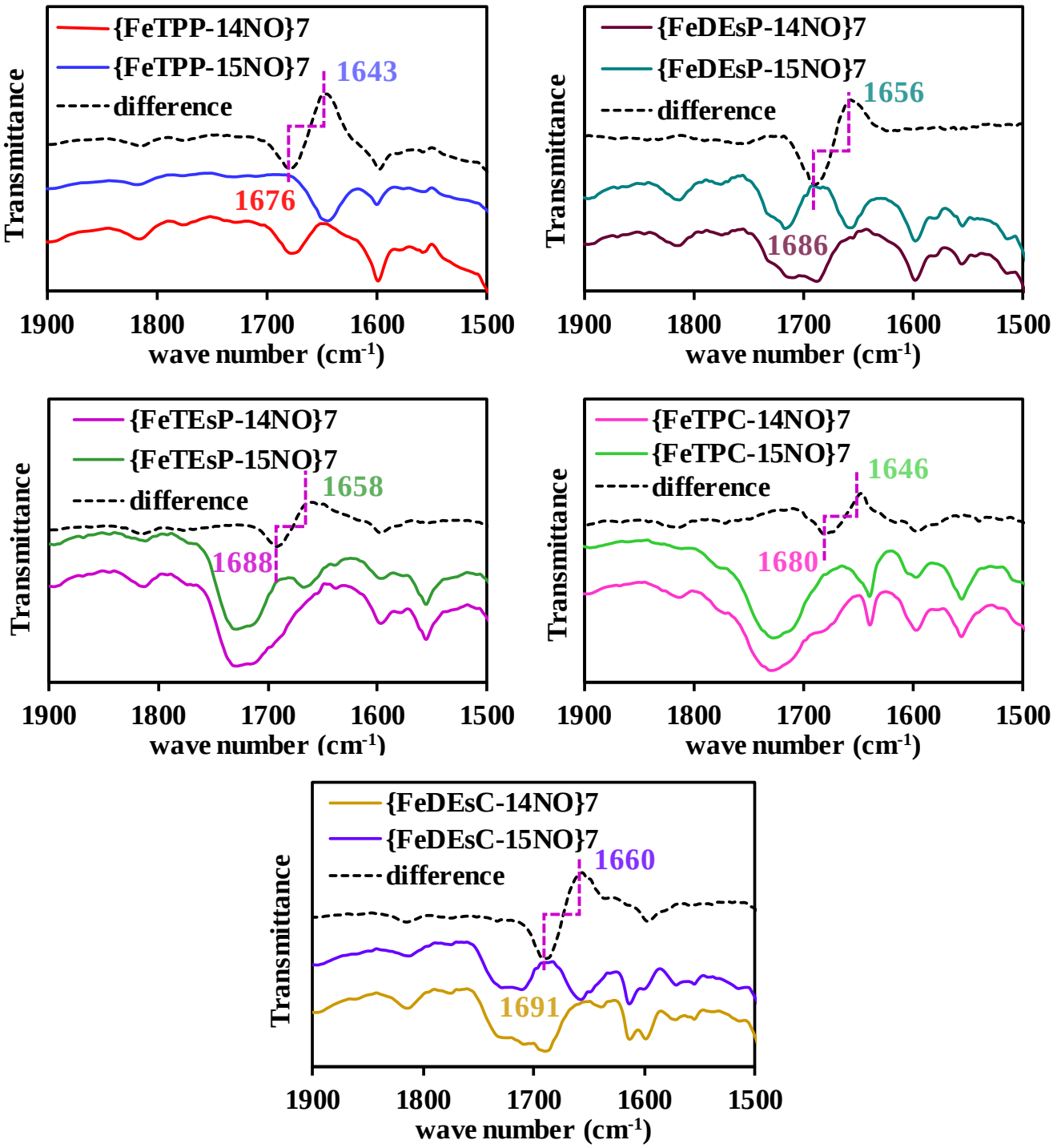

Figure 6. FTIR data of the $\{FeNO\}^7$ adducts in dichloromethane at room temperature.

View Article Online
DOI: 10.1039/D0SC01625J

The displacement of the bound NO from the N-methylimidazole bound six-coordinated $\{FeNO\}^7$ species by NO_2^- was investigated using absorption spectroscopy (See SI, section 8). The K_d for the process ($Fe^{II} - NO + NO_2^- \rightleftarrows Fe^{II} - NO_2^- + NO$) was determined to be 0.09 for FeTPP and 0.46 for FeDEsC (Table 1). The higher K_d for FeDEsC, relative to FeTPP, translated to a ΔG difference of ~1 Kcal/mol and correlated very well with its stronger N-O stretching frequency and demonstrated clearly how the EWG and saturation of the porphyrin ring aid the displacement of NO by NO_2^-, as proposed in Cd_1NiR. A similar effect was observed on the displacement rate of NO by pyridine in $\{FeNO\}^7$ complexes in a series of iron porphyrins, where the octa-halogenated derivative of TPP was ~10^6 times faster than that of FeTPP.[22]

Spectroelectrochemistry was used to access the N-O vibrations of the $\{FeNO\}^6$ and $\{FeNO\}^8$ species (Table 1, Figure S26-S28). The N-O vibrations for the six-coordinate $\{FeNO\}^6$ for FeTPP, FeDEsP, and FeTEsP were obtained at 1914 cm^{-1}, 1923 cm^{-1}, and 1927 cm^{-1}, respectively (Figure S27). The higher N-O vibration for the porphyrins containing EWGs relative to FeTPP mirrored the trend observed for the corresponding $\{FeNO\}^7$ species. The N-O vibrations for both five and six-coordinate $\{FeNO\}^6$ species of FeTPC and FeDEsC could not be obtained, which was consistent with the irreversible CV observed for these species indicating that these $\{FeNO\}^6$ species dissociate within the time scale of the experiment (Figure S23B and S27). The inability to identify five-coordinate $\{FeNO\}^6$ species of FeDEsP and FeTEsP again suggested the formation of a labile $\{FeNO\}^6$ adduct. The N-O vibrations for the $\{FeNO\}^8$ species could be observed for FeTEsP and FeDEsC at 1550 cm^{-1} and 1537 cm^{-1}, respectively (Figure S28, Table S2). The values obtained were consistent with the previously reported values for the five-coordinate $\{FeNO\}^8$ porphyrins.[54, 60, 61] Note that the frequencies were much higher than the value reported for FeTPP at 1496 cm^{-1}.[43] Here, too, the inclusion of the EWG and saturation together lead to a substantial increase in the N-O vibration indicating a weakening of the Fe-NO bonding. Thus, the FTIR data for the $\{FeNO\}^6$, $\{FeNO\}^7$, and $\{FeNO\}^8$ species all showed that the inclusion of EWG and saturation at the periphery of the porphyrin macrocycle substantially weakened the Fe-NO bonding.

View Article Online
DOI: 10.1039/D0SC01625J

Table 1. Properties of {FeNO}$^{6//7/8}$ species for the synthetic porphyrins

	{FeNO}^{6}	⇔	{FeNO}^{7}	⇔	{FeNO}^{8}	K_d[e]
	ν_{N-O}[a] 5C (6C)	$E^{0,b}$	ν_{N-O} 5C (6C)	E^0	ν_{N-O} 5C (6C)	
FeTPP-NO	1844 (1914)	0.20	1676 (1626)	-1.41	1496[43]	0.09±0.05
FeDEsP-NO	c (1923)	0.34	1686 (1641)	-1.24	c	0.20±0.04
FeTEsP-NO	c (1927)	0.38	1688 (1646)	-1.14	1550	0.23±0.02
FeTPC-NO	d	-0.04[d]	1680 (1635)	-1.51	c	0.13±0.04
FeDEsC-NO	d	0.10[d]	1691 (1633)	-1.42	1537	0.46±0.04

a. stretching frequency in cm^{-1}, b. Potentials are reported vs Fc$^+$/Fc in dichloromethane, c. Not observed and d. irreversible cathodic waves, e. $Fe^{II} - NO + NO_2^- \rightleftarrows Fe^{II} - NO_2^- + NO$

A plot of the experimentally observed N-O vibrations (Table 1) with ln(K_d) for the series of complexes investigated here showed a reasonably linear correlation (Figure 7) in line with the linear correlation observed between ν(N-O) and ln(k_{off}) (Figure 2). Thus, the electronic structure responsible for the correlation in the enzyme active site was captured in the series of porphyrins used here – primarily the competitive back-bonding between porphyrin π^* and NO π^*-orbitals adding credence to the use of electron-withdrawing –COOEt group to mimic the keto-group in heme d_1. The K_d was larger for {Fe-NO}^{7} species with higher ν(N-O) frequency. The stronger back-bonding with the porphyrin π^* will reduce back-bonding to the NO π^* thus tuning its pK_a. It is conceivable that this will affect the thermodynamics of the PCET to {FeNO}^{7} to form {FeHNO}^{8}.

View Article Online
DOI: 10.1039/D0SC01625J

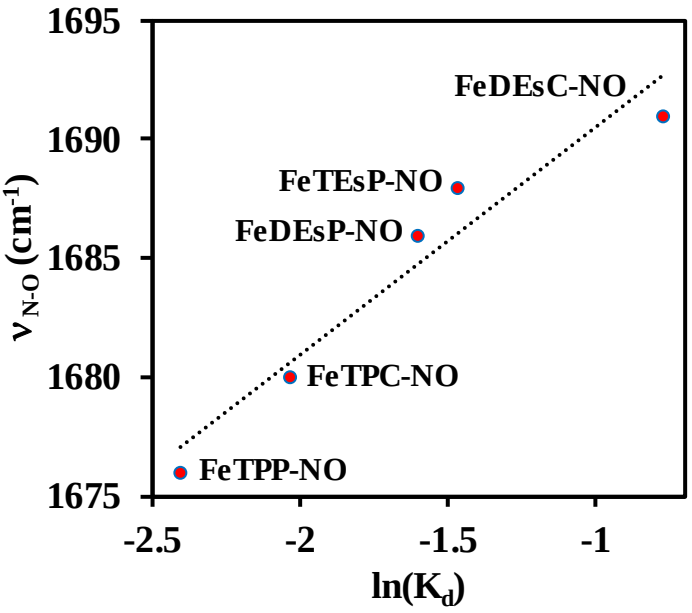

Figure 7: Correlation between experimentally measured N-O stretching frequency and NO dissociation constant

4. PCET to {FeNO}^{7}

The {FeNO}^{7} species of CcNiR, with heme *c*, accepts $1H^+/1e^-$ to form {FeHNO}^{8} on its way to form NH_4^+ without releasing any intermediate species and does not dissociate NO.[9] The lower N-O stretch in {FeNO}^{7} of heme *c* (1651-1671 cm^{-1})[62], in general, was suggestive of a weak NO dissociation in CcNiR. But, for a facile PCET, the BDFE of the N-H bond in {FeNHO}^{8} should be high as well.[63] The BDFE of the N-H bond in {FeHNO}^{8} species can be calculated using the following equation:[64]

$$BDFE_{NH} = 1.37\ pK_a + 23.06\ E^\circ + C$$

Where, the pK_a was that of {FeNO}^{8} species, which was calculated from the change in Gibb's free energy, ΔG° of the protonation equilibrium between {FeNO}^{8} and {FeHNO}^{8}. The E° represents the one-electron reduction potential of {FeNO}$^{7/8}$ redox process, which was directly obtained from the cyclic voltammogram. C is a constant which depends on the solvent.[64] The pK_a of the {FeNO}^{7} species was difficult to determine as the protonation leads to an irreversible reaction.[42] Thus, the ΔG° of protonation was computed using DFT calculations. The $BDFE_{NH}$ values estimated using these were normalized relative to FeDEsC-NO which was set at 0 Kcal/mol (Table 2). These calculations indicated that the protonation of {FeNO}^{8} species gradually became less favorable from FeOEP to FeOEPone to Fe(2,4-OEPdione). It was consistent with the previously reported trend for nitrite reduction to ammonia, using moderately strong acids like phenols, under controlled potential electrolysis i.e., the rate of the reaction: FeOEP> FeOEPone > Fe(2,4-OEPdione), where the protonation of {FeNO}^{8} species was proposed to be the rate-limiting step.[42]

View Article Online
DOI: 10.1039/D0SC01625J

Table 2. Values of pK_a, E^o, and $BDFE_{NH}$ relative to FeDEsC-NO

Complexes	ΔpK_a	ΔE° (mV)	$\Delta BDFE_{NH}$ (Kcal/mol)
FeTPP-NO	1.57	10	2.38
FeDEsP-NO	-0.32	180	3.71
FeTEsP-NO	-3.12	280	2.18
FeTPC-NO	1.92	-90	0.56
FeDEsC-NO	-	-	-
FeOEP-NO	5.36	-70	5.73
FeOEPone-NO	0.91	140	4.47
Fe(2,4-OEPdione)-NO	-1.76	260	3.58

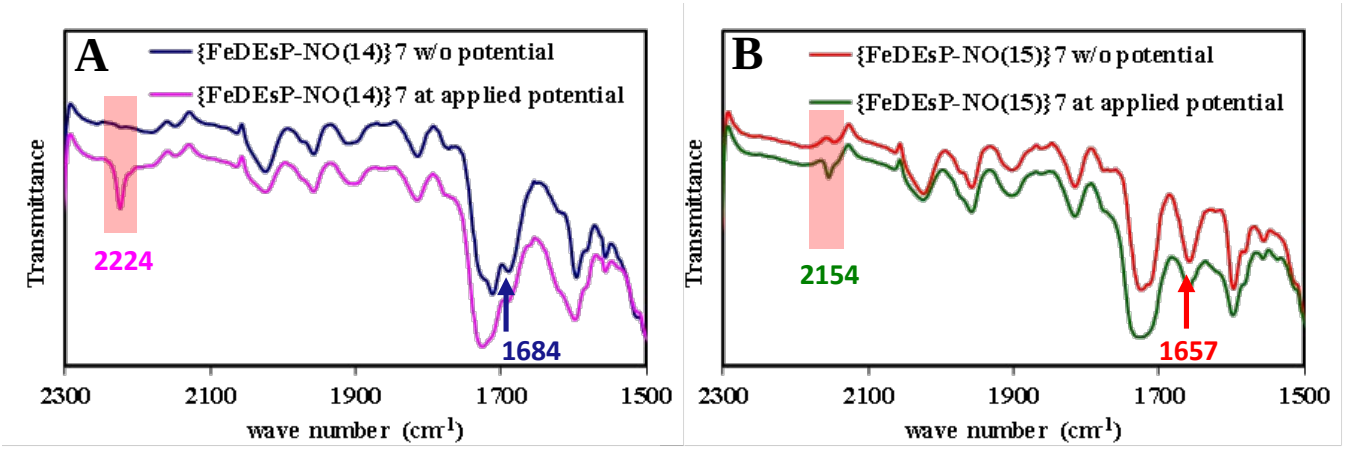

Figure 8. Formation of N_2O during electrolysis of $\{FeDEsP\text{-}NO\}^7$ at -1.31 V (vs Fc^+/Fc). On applying potential, N_2O is generated ($\nu_{N\text{-}O\ (14/15)}$: 2224/2154 cm^{-1}), with the expanse of $\{FeDEsP\text{-}NO\}^7$ peaks. A) in the presence of ^{14}NO and B) in the presence of ^{15}NO.

Comparing the ΔG° for PCET to the $\{FeNO\}^7$ species of FeDEsC-NO and FeDEsP-NO (without saturated pyrroles), the major contribution to the difference was derived from the of the $\{FeNO\}^{7/8}$ redox process. The E° was increased by ~180 mV in FeDEsP-NO, making the reduction more facile. As a result, the $BDFE_{NH}$ of $\{FeHNO\}^8$ species of FeDEsP-NO was increased by ~3.71 Kcal/mol, relative to FeDEsC-NO, suggesting that the $\{FeNO\}^7$ species of FeDEsP-NO should be more prone to undergo PCET reaction than FeDEsC-NO. Gratifyingly, during the electrochemical reduction of FeDEsP-NO, it generated N_2O

View Article Online
DOI: 10.1039/D0SC01625J

in the presence of methanol as the proton source. This was evidenced by the growth of a vibrational band at 2224 cm^{-1} as cathodic potential was applied (Figure 8A), which shifted to 2154 cm^{-1} when ^{15}NO was used (Figure 8B). The formation of N_2O from NO can be mediated by $\{FeHNO\}^8$ which is difficult to characterize under electrochemical conditions.[65] Alternatively, when $\{FeDEsP\text{-}NO\}^7$ was reduced chemically by cobaltocene in presence of methanol and PPh_3, it readily generated $Ph_3P{=}O$ and $Ph_3P{=}NH$ (see SI, section 10, Figure S33-35), suggesting the generation of HNO in the solution. This can only happen if the reaction proceeds through the PCET process forming a $\{FeHNO\}^8$ species.[66] Note that these results do not imply that FeDEsP mirrored the reactivity of CcNiR because CcNiR does not release any HNO, it generates NH_4^+ via $\{FeHNO\}^8$ without releasing HNO or N_2O. The fact that FeDEsP-NO could produce HNO from a weak proton donor while the NO could be displaced by NO_2^- in FeDEsC-NO, suggested that the electronic structure of the porphyrin ring resulting from EWG and saturation can discriminate NO release vs PCET to a $\{FeNO\}^7$ species under physiological conditions.

Discussion

It has been proposed that CcNiR undergoes two consecutive PCET reactions on the $\{FeNO\}^6$ intermediate. The first PCET forms a $\{FeNO\}^7$ species (with protonation of Arg_{114} residue) which subsequently generates $\{FeHNO\}^8$ species through another PCET process, releasing only a trace amount of the $\{FeNO\}^7$ intermediate.[11, 67] In contrast, Cd_1NiR undergoes an electron transfer (ET) from cytochrome *c*, forming the $\{FeNO\}^7$ intermediate, which releases NO rapidly (k_{off} ~200 s^{-1}).[13, 19] There is an extensive debate on whether the NO is released from the ferric state or the ferrous state of the NO adduct.[1, 68] Recent data suggest that it is likely that NO is released from the ferrous, $\{FeNO\}^7$ state.[2, 13, 59] The fast release of NO from $\{FeNO\}^7$ intermediate may be attributed to a weak Fe-NO bonding in the ferrous nitrosyl adduct formed. The higher N-O stretching frequencies in the $\{FeNO\}^n$ (n=6,7, and 8) species of FeTEsP and FeDEsC suggested weak Fe-NO bonding, i.e., four electron-withdrawing ester groups or two ester group with two saturated carbon centers had an almost similar effect. Thus, heme *d_1*, which had two EW-keto groups and two saturated pyrrolic carbons, was likely to have a weaker Fe-NO bond relative to heme *c*, which has neither. A weaker Fe-NO in FeDEsC is associated with a large K_d for NO_2^- replacement relative to FeTPP consistent with the strong linear correlation between $\nu_{N\text{-}O}$ and K_d observed for both enzymatic and synthetic systems. Similarly, a weaker Fe-NO in heme *d_1* active site of Cd_1NiR, evident from a higher $\nu_{N\text{-}O}$, should result in higher NO (product) K_d, relative to NO_2^- (substrate). It might be envisaged that due to the ruffled nature of isobacteriochlorin ring in heme *d_1*, they form weak $\{FeNO\}^7$ species. But calculations of the ruffling parameters[69] suggested maximum ruffling was present in $\{FeTPC\text{-}NO\}^7$ species, which possess a chlorin ring (see SI, section 9), and had a relatively strong Fe-NO bond.

View Article Online
DOI: 10.1039/D0SC01625J

The ΔG° for PCET to the $\{FeHNO\}^8$, the competing reaction to NO release, was affected by both E° and pK_a of the $\{FeNO\}^7$ species. Between FeDEsC-NO and FeTPC-NO, where the latter was devoid of EWGs, the pK_a of $\{FeNO\}^8$ species increased by 1.92 unit (Table 2), but it lowered the E° of $\{FeNO\}^{7/8}$ redox process by ~90 mV (Table 2), making the PCET to the $\{FeNO\}^7$ species of FeTPC-NO slightly favorable, relative to FeDEsC-NO. By omitting both saturation and EWGs (FeTPP-NO), the E° decreased while the pK_a of $\{FeNO\}^8$ species increased which resulted in higher $BDFE_{NH}$ of the $\{FeHNO\}^8$ species but not as high as of FeDEsP-NO. In the case of FeTEsP-NO, where the saturation was absent but two more EWGs were present (relative to FeDEsC-NO), the E° increased by ~280 mV but the pK_a of $\{FeNO\}^8$ species becomes too low to be protonated, resulting $BDFE_{NH}$ lower than FeTPP-NO. Therefore, for a facile PCET, there needs to be a balance between E° and pK_a, which was attained here in FeDEsP-NO. This model was equally applicable to FeOEP system, where the high $BDFE_{NH}$ was due to the greater pK_a of the $\{FeNO\}^8$ species. Introducing EW-keto groups increased the E° but at the expense of the pK_a of $\{FeNO\}^8$ species (Table 2), resulting in a gradual decrease in $BDFE_{NH}$. However, it should also be noted that $\{FeHNO\}^8$ species is not very stable due to the disproportionation of Fe-HNO unit. The $\{FeHNO\}^8$ species could only been stabililized either with steric protection (bis-picket fence porphyrin[46] or globin chain in hemoglobin[44, 45]) or in a highly electron-rich porphyrin like FeOEP ($\nu_{NO/\{FeNO\}^7}$ = 1665 cm^{-1}). [70, 41, 71, 72] Hence, it is not surprising, that $\{FeHNO\}^8$ species in electron-deficient octabromo[tetrakis(pentafluorophenyl)]porphyrin, Fe(TFPPBr$_8$)(NO) ($\nu_{NO/\{FeNO\}^7}$ = 1726 cm^{-1})[54] could not be isolated. The weak $BDFE_{NH}$ and weaker $\{FeNO\}^7$ adduct likely biases the FeDEsC (which have two EWGs along with two saturated pyrrolic carbons, like heme *d*$_1$ in the active site of Cd_1NiR) for NO dissociation. On the contrary, stronger $BDFE_{NH}$ driven by a favourable balance between pK_a (due to better back-bonding to the NO π^*-orbitals) and E° is responsible for facile PCET to $\{FeNO\}^7$ to produce $\{FeHNO\}^8$ which is necessary to eventually release NH_4^+ in CcNiR.

Conclusion

In summary, the results on structural variants of iron-porphyrins suggested that Cd_1NiR does not proceed with the PCET process to form $\{FeHNO\}^8$ intermediate, due to its lower $BDFE_{NH}$ arising from the weaker back-donation from heme *d*$_1$ where the EWGs and sp^3 peripheral carbons enhance competitive back-bonding from the iron to the porphyrinoid π^* and NO π^*-orbitals. The weaker back-bonding to the bound NO results in weaker Fe-NO bond and hence, it releases NO. In CcNiR, on the other hand, heme *c* has greater back-bonding to the NO from iron, which strengthens the Fe-NO bond and tunes the pK_a allowing to undergo PCET to form $\{FeHNO\}^8$ species, which is crucial for the further reactions to release NH_4^+.

View Article Online
DOI: 10.1039/D0SC01625J

Experimental Details

Materials: All reagents were of the highest grade commercially available. Iodine, trifluoroacetic acid (TFA), 2,3-dichloro-5,6-dicyano-1,4-benzoquinone (DDQ), ethanol, aqueous ammonia solution, ceric ammonium nitrate (CAN), sarcosine, potassium *tert*-butoxide, benzaldehyde, magnesium sulphate, *p*-toluenesulphonic acid (PTSA), *p*-toluenesulfonylmethyl isocyanide (TosMIC), phosphorus oxychloride ($POCl_3$), dichloroethane (DCE), propionic acid were purchased from Spectrochem Ltd. Diethyl ether, Tetrahydrofuran (THF), Acetonitrile, Dichloromethane, and Toluene were purchased from RANKEM Ltd., paraformaldehyde, anhydrous Ferrous bromide ($FeBr_2$), 2,4,6-Collidine, Tetrabutylammonium hexafluophosphate ($TBAPF_6$) were purchased from Sigma-Aldrich chemical company. Na_2SO_4, Zinc acetate were purchased from MERCK and used without any further purification. Unless otherwise mentioned all reactions were performed at room temperature. The column chromatography was performed with silica gel (mesh size: 60-100, 100-200 and 230-400) and neutral Alumina, preparative TLC was performed with Silica gel GF-254 (~13% $CaSO_4$, 0.5 H_2O binders with fluorescent indicator). These were purchased from SRL Pvt. Ltd. THF was dried using K-metal in the presence of benzophenone until the colour of benzophenone turned intense bluish-green. Toluene was dried using Na-metal in the presence of benzophenone until the colour of benzophenone turned intense blue. MeOH was first dried like toluene using sodium after that it was distilled from Mg-cake. DCM and chloroform were distilled with both anhydrous $CaCl_2$ followed by CaH_2.

Instrumentation: All electrochemical experiments were performed using CH Instruments (model CHI700E and CHI710D Electrochemical Analyzer). Biopotentiostat, reference electrode (standard single-junction silver/silver chloride filled with 4M KCl with AgCl solution) were purchased from CH Instruments. The absorption spectra were measured in the SHIMADZU spectrograph (UV-2100). The aerobic and anaerobic cuvettes were purchased from Starna Scientific. The FT-IR data were measured on the Shimadzu FTIR 8400S instrument. The CaF_2 windows for IR spectroscopy were purchased from Sigma Aldrich. The anaerobic setup for IR spectroscopy was purchased from PerkinElmer. The optically transparent thin-layer electrochemical cell (OTTLE) was purchased from the University of Reading for spectroelectrochemistry. All the NMR spectra were recorded on the Bruker DPX-300, Bruker DPX-400 or DPX-500 spectrometer at room temperature. The mass spectra were recorded by the QTOF Micro YA263 instrument. Resonance Raman data were collected using a Trivista 555 spectrograph (Princeton Instruments) and using 413.1 nm excitation from a Kr^+ laser (Coherent, Sabre Innova SBRC-DBW-K). The X-band EPR spectra were recorded on a JEOL instrument. X-ray single-crystal data were collected at 120 K using radiation on a SMART APEX diffractometer equipped with CCD detector. Data collection, data reduction, structure solution refinements were carried out using the software package of APEXIII.

View Article Online
DOI: 10.1039/D0SC01625J

The structure was solved by the direct method and refined in a routine manner. The non-hydrogen atoms were treated anisotropically. All the hydrogen atoms were located on a difference Fourier map and refined.

Electrochemical Measurements: Since $\{FeNO\}^8$ readily react with a trace amount of water present in the solvents,[43] every solvent used in electrochemical measurements were first dried following the aforementioned protocol. After that, they had been super-dried with activated 4Å molecular sieves and kept inside the glove box for 1 week. Nitrosyl adduct of the five complexes (FeTPP, FeDEsP, FeTEsP, FeTPC, and FeDEsC) were considered for electrochemical analysis. All CV data were collected under anaerobic conditions in a custom made electrochemical cell. 6 ml of NO-complex (concentration: 1 mM) was taken in presence of 100 mM $TBAPF_6$ as supporting electrolyte. The glassy carbon electrode was taken as a working electrode, standard single-junction silver/silver chloride filled with 4M KCl with AgCl solution as the reference electrode and a Pt electrode was taken as the counter electrode. Ferrocene (Fc) was used as an internal reference and the potential scale is normalized with respect to the potential of the Fc^+/Fc couple. The potential was swept starting from 0V to a positive potential (oxidation) followed by negative potential (reduction), except for FeDEsC-NO, here sweeping positive potentials, lead to irreversible CV. Hence, for this, the potential was swept from 0V to negative potential (reduction) followed by positive potential (oxidation).

NO complex preparation: Dry degassed NO gas was generated upon the dropwise addition of a deaerated saturated solution of sodium nitrite to the deaerated 6M H_2SO_4. The gas was passed through two 4N KOH solution bubbler followed by one concentrated H_2SO_4 solution. The solution of each complex was reduced by 0.5 equivalent Na_2S solution (in methanol) inside a glove box, sealed properly and kept out of the box. NO gas was purged through the samples (kept in an ice bath to reduce solution evaporation) for 5 mins. The vials were tightly sealed and used for further investigations. NO complexes were also prepared using Ph_3CSNO (as well as $Ph_3CS^{15}NO$), which were prepared through reported procedures.[73, 74] To the reduced samples, 1 equivalent of Ph_3CSNO in THF/DCM (whichever required) was added. The vials were perfectly sealed and used for further investigations. The detailed characterization of the five and six-coordinated N-methylimidazole bound $\{FeNO\}^7$ adducts are given in the main text and the supporting informations (Figure S24A-B, S24A-C, Table S1).

FTIR data collection: DCM/THF solution of the complexes were injected in the anaerobic FTIR setup or OTTLE cell and tightly sealed inside a glove box. The cell was removed from the box and data collected. Spectroelectrochemistry was performed using the OTTLE cell connecting with the electrochemical analyzer. The sample solution contained 100 mM $TBAPF_6$ as a supporting electrolyte. The FTIR spectra were taken at different time intervals under electrolysis conditions.

View Article Online
DOI: 10.1039/D0SC01625J

UV-Vis absorption data collection: For all anaerobic data were collected taking the samples from the glove box in a tightly sealed anaerobic cuvette. The cuvette was removed from the box and data collected. The background was corrected before the experiments, by an identical amount of solvent mixture.

Computational Details: All calculations were performed at the IACS computer cluster using Gaussian 03 software.[75] BP86 functional reproduced better agreement with the experimental frequencies and hence further calculations were performed with that functional. A mixed basis set with 6-311g* on Fe and 6-31g* on C, O, N and H atoms were used for optimization.[76, 77] For the final energy and ground-state calculations, a 6-311+g* basis set was used on all atoms. The solvent effect was corrected using the Polarizability Continuum Model (PCM).[78] For all complexes spin-unrestricted schemes have been adopted which distinguishes between α and β-spin orbitals. Frequency calculations were performed using the basis set used for optimization, and no negative frequencies were found for the structures reported.

Synthetic details

The FeTPP, FeTPC, FeDEsP and FeDEsC complexes were synthesized following the reported procedures.[23] The synthetic procedure of FeTEsP is described below:

Diethyl 1H-pyrrole-3,4-dicarboxylate (DEspyr): 110 ml dry THF was added to Potassium tertiary butoxide (15.57 g, 138.7 mmol) in a flask attached to a Schlenk line under N_2 atmosphere. A solution of tosyl methyl isocyanide (TosMIC) (13.5 g, 69.4 mmol) and diethyl fumarate (10 ml, 69.4 mmol) in 60 ml dry THF was prepared and added dropwise to the flask keeping in the ice water bath. Stirring was continued for 6 to 7 hours at room temperature. Then THF was evaporated and the reaction was quenched using saturated NH_4Cl solution. The mixture was worked up with ethyl acetate and dried over Na_2SO_4 and evaporated through a rotary evaporator. Purification was done by recrystallization from methanol. Crystals obtained were washed with cold ethyl acetate. ^1H NMR ($CDCl_3$): δ (ppm) 1.30 (t, 6H), 4.25 (q, 4H), 7.38 (d, 2H), 10.57 (bs, 1H). ^{13}C {^1H} NMR ($CDCl_3$): δ (ppm) 14.33, 60.26, 115.39, 126.59, 166.42. ESI-MS (Positive ion mode, CH_3CN): m/z 234.05 (100%; $[M+Na]^+$), 212.09 (45%; $[M+H]^+$), 250.05 (30%;$[M+K]^+$)

Tetraethyl 2,2'-(phenylmethylene)bis(1H-pyrrole-3,4-dicarboxylate) (TEsbpyr): *p*-tolunesulphonic acid (0.89 g, 4.7 mmol) and $MgSO_4$ (0.23 g, 1.9 mmol) were taken in a flask. Benzaldehyde (194 µl, 1.9 mmol) was added to it under N_2 atmosphere. The solid mixture was heated under vacuum until yellow colouration. Then THF (2 ml) was added and it was heated for 5 minutes. Then a solution of DEsPyr (1 g, 4.7 mmol) in dry $CHCl_3$ was added to it. The solution was refluxed for 5 hours. The reaction was quenched using concentrated NaOH solution and was worked up with dichloromethane. The organic layer was dried over Na_2SO_4, evaporated through a rotary evaporator and was dissolved in a minimum amount

View Article Online
DOI: 10.1039/D0SC01625J

of DCM and charged on GF-254 silica gel preparative TLC plate and eluted with 30% ethyl acetate-hexane mixture. The product band was scratched off and extracted with ethyl acetate. ^{1}H NMR ($CDCl_3$): δ (ppm) 1.14 (t, 6H), 1.33 (t, 6H), 4.03 (q, 4H), 4.26 (q, 4H), 6.27 (s, 1H), 6.88 (d, 2H), 7.22 (m, 5H), 10.64 (bs, 2H), 1.26, 2.04, 4.12 (for EtOAc). ^{13}C {^{1}H} NMR ($CDCl_3$): δ (ppm) 13.75, 14.26, 40.51, 60.11, 61.08, 113.21-139.15, 164.01, 167.00. ESI-MS (Positive ion mode, CH_3CN): m/z 533.35 (100%; $[M+Na]^+$), 549.34 (45%;$[M+K]^+$), 511.38 (35%; $[M+H]^+$).

Tetraethyl 5,5'-(phenylmethylene)bis(2-formyl-1H-pyrrole-3,4-dicarboxylate) (TEsbpyr-dial): $POCl_3$ (450 µL, 4.8 mmol) was added slowly to DMF (380 µL, 4.8 mmol) taken in a flask, kept in an ice bath to form the Vilsmeier-Haack reagent. The reagent was dissolved in DCE, degassed and then added dropwise to another flask containing TEsbpyr (250 mg, 0.48 mmol) in DCE keeping the flask on ice bath under N_2 atmosphere. The reaction mixture was degassed for 15 minutes and then refluxed for 5 hours. The reaction was monitored by TLC after charring the TLC plate using 2,4-DNP solution. The reaction was then quenched by adding a saturated solution of sodium acetate and worked up with dichloromethane. The organic layer was dried over Na_2SO_4, evaporated through a rotary-evaporator and purified by column chromatography on silica gel (100-200 mesh) with EtOAc: toluene (1:10). ^{1}H NMR($CDCl_3$): δ (ppm) 1.21 (t, 6H), 1.39 (t, 6H), 4.15 (q, 4H), 4.40 (q, 4H), 6.72 (s, 1H), 7.01 (d, 2H), 7.26 (m, 5H), 9.92 (s, 2H), 11.35 (bs, 2H). ^{13}C {^{1}H} NMR ($CDCl_3$): δ (ppm) 13.97, 14.23, 29.63, 40.43, 114.19-139.67, 163.12, 164.87, 180.80. ESI-MS (Positive ion mode, CH_3CN): 589.66 (75%, $[M+Na]^+$) , 605.65 (25%, $[M+K]^+$), 567.65 (10%,$[M+H]^+$).

5-phenyldipyrromethane: 5-phenyldipyrromethane was synthesized following the reported protocol.[79]

Tetraethylesterdiphenylporphyrin (TEsP): TEsbpyr-dial (200 mg, 0.36 mmol) and 5-phenyldipyrromethane (79.5 mg, 0.36 mmol) was taken in a round bottom flask. Propionic acid (70 ml) was added and the system was refluxed for 30 minutes. The acid was distilled out from the reaction mixture. The solid product obtained was washed with warm water to remove the remained acid. It was then dissolved in dichloromethane and dried over Na_2SO_4, evaporated through a rotary-evaporator. Polypyrrole formed during the reaction was removed through column chromatography on silica gel (100-200 mesh) with EtOAc-hexane (1:4). The product was purified by second column chromatography using 0.1% dichloromethane-methanol (99:1) mixture. ^{1}H NMR($CDCl_3$): δ (ppm) -2.31 (br s, 1H), -2.05 (br s, 1H), 1.38 (t, 6H), 1.61 (t, 6H), 4.05 (t, 4H), 4.76 (q, 4H), 7.64-8.20 (m, 10H), 8.97 (d, 2H), 9. 36 (d, 2H), 11.23 (s, 2H). ^{13}C {^{1}H} NMR ($CDCl_3$): δ (ppm) 13.92, 14.56, 22.83, 29.50, 29.84, 61.96, 62.10, 106.44, 119.45-141.19, 146.99, 151.09, 164.70, 166.85. ESI-MS (Positive ion mode, CH_3CN): m/z 751.11 (50 %, $[M+H]^+$).

View Article Online
DOI: 10.1039/D0SC01625J

FeTEsP: TEsP (30 mg, 0.04 mmol) was dissolved in dry THF (15 ml), 2,4,6-collidine (20.8 µL, 0.16 mmol) was added under N_2 atmosphere to generate the porphyrin base. Then $FeBr_2$ (34.5 mg, 0.16 mmol) was added to it. The reaction mixture was stirred for 10 hrs at room temperature and the progress of the reaction was monitored by TLC. On full conversion, THF was evaporated using a rotary evaporator and workup was done using dichloromethane and HCl (to remove excess $FeBr_2$ as $FeCl_4^-$). The organic layer was dried over Na_2SO_4, evaporated through a rotary-evaporator and purified by column chromatography on silica gel (100-200mesh) with 3.5% dichloromethane-methanol (96.5:3.5). ^{1}H NMR-Paramagnetic ($CDCl_3$): δ (ppm) 75.99, 79.94, 81.83. ESI-MS (Positive ion mode, CH_3CN): m/z 804.86 (100 %, $[M]^+$).

ZnTEsP: TEsP (30 mg, 0.04 mmol) was dissolved in dry THF (15 ml), 2,4,6-collidine (20.8 µL, 0.16 mmol) was added to generate the porphyrin base. Then $Zn(OAc)_2$ (29.35mg, 0.16 mmol) was added to it. The reaction mixture was stirred for 10 hrs and the progress of the reaction was monitored by TLC. On full conversion, THF was evaporated and it was purified by column chromatography on silica gel (100-200 mesh) with 0.3% dichloromethane-methanol (99.7:0.3). ^{1}H NMR ($CDCl_3$): δ (ppm) -2.31.07 (t, 3H), 1.38 (t, 3H), 3.28 (q, 2H), 4.34 (q, 2H), 6.94-8.21 (m, 10H), 8.95 (d, 2H), 9.25 (d, 2H), 10.66 (s, 2H). ^{13}C {^{1}H} NMR ($CDCl_3$): δ (ppm) 13.54, 14.42, 61.42, 61.70, 106.79, 119.79-144.89, 151.35, 153.86, 164.47, 167.10. ESI-MS (Positive ion mode, CH_3CN): m/z 835.04 (100 %, $[M+Na]^+$), 812.09 (80%, [M]).

ASSOCIATED CONTENT

Supporting Information

The Supporting Information is available free of charge on the ACS Publications website at pubs.acs.org.

Additional NMR, mass, UV−vis, and FTIR data and coordination of the DFT-optimized structures (PDF).

Accession Codes

CCDC 1854376 (FeDEsP) , 1854377 (ZnDEsC) and 1959224 (ZnTEsP) contain the supplementary crystallographic data for this paper. These data can be obtained free of charge via www.ccdc.cam.ac.uk/data_request/cif, or by emailing data_request@ccdc.cam.ac.uk, or by contacting The Cambridge Crystallographic Data Centre, 12 Union Road, Cambridge CB2 1EZ, UK; fax: +44 1223 336033.

AUTHOR INFORMATION

View Article Online
DOI: 10.1039/D0SC01625J

Corresponding Author

Abhishek Dey, Email: icad@iacs.res.in.

ORCID

Abhishek Dey: 0000-0002-9166-3349

Sk Amanullah: 0000-0003-3288-5942

Present Addresses

School of Chemical Sciences, Indian Association for the Cultivation of Science, 2A & 2B Raja SC Mullick Road, Kolkata, India – 700032

Author Contributions

Notes

The authors declare no competing financial interests.

ACKNOWLEDGMENT

This research is funded by the Council of Scientific and Industrial Research (CSIR) Grant 01(2874)/17/EMR-II and Department of Science and Technology grant SERB/EMR/008063. S.A. acknowledges CSIR-SRF. Ms. Paramita Saha is greatly acknowledged for her help in synthesis.

REFERENCES

1. B. A. Averill, *Chemical Reviews*, 1996, **96**, 2951-2964.
2. L. B. Maia and J. J. G. Moura, *Chemical Reviews*, 2014, **114**, 5273-5357.
3. C. Moreno-Vivián, P. Cabello, M. Martínez-Luque, R. Blasco and F. Castillo, *Journal of Bacteriology*, 1999, **181**, 6573.
4. , !!! INVALID CITATION !!! 4, 5.
5. S. Rinaldo, G. Giardina, N. Castiglione, V. Stelitano and F. Cutruzzolà, *Biochemical Society Transactions*, 2011, **39**, 195.
6. Y. Shiro, *Biochimica et Biophysica Acta (BBA) - Bioenergetics*, 2012, **1817**, 1907-1913.
7. K. Brown, K. Djinovic-Carugo, T. Haltia, I. Cabrito, M. Saraste, J. G. Moura, I. Moura, M. Tegoni and C. Cambillau, *Journal of Biological Chemistry*, 2000, **275**, 41133-41136.
8. S. Teraguchi and T. C. Hollocher, *Journal of Biological Chemistry*, 1989, **264**, 1972-1979.
9. O. Einsle, A. Messerschmidt, R. Huber, P. M. H. Kroneck and F. Neese, *Journal of the American Chemical Society*, 2002, **124**, 11737-11745.
10. S. J. George, J. W. A. Allen, S. J. Ferguson and R. N. F. Thorneley, *Journal of Biological Chemistry*, 2000, **275**, 33231-33237.
11. D. Bykov and F. Neese, *JBIC Journal of Biological Inorganic Chemistry*, 2012, **17**, 741-760.
12. K. Kobayashi, A. Koppenhöfer, S. J. Ferguson, N. J. Watmough and S. Tagawa, *Biochemistry*, 2001, **40**, 8542-8547.
13. M. Radoul, D. Bykov, S. Rinaldo, F. Cutruzzolà, F. Neese and D. Goldfarb, *Journal of the American Chemical Society*, 2011, **133**, 3043-3055.
14. S. Rinaldo, M. Brunori and F. Cutruzzolà, *Biochemical and Biophysical Research Communications*, 2007, **363**, 662-666.
15. C. E. Cooper, *Biochimica et Biophysica Acta (BBA) - Bioenergetics*, 1999, **1411**, 290-309.
16. T. K. Das, E. K. Wilson, F. Cutruzzolà, M. Brunori and D. L. Rousseau, *Biochemistry*, 2001, **40**, 10774-10781.
17. X. J. Zhao, V. Sampath and W. S. Caughey, *Biochemical and Biophysical Research Communications*, 1994, **204**, 537-543.
18. J. C. Maxwell and W. S. Caughey, *Biochemistry*, 1976, **15**, 388-396.
19. S. Rinaldo, Katharine A. Sam, N. Castiglione, V. Stelitano, A. Arcovito, M. Brunori, James W. A. Allen, Stuart J. Ferguson and F. Cutruzzolà, *Biochemical Journal*, 2011, **435**, 217.
20. J. S. Olson and G. N. Phillips, *Journal of Biological Chemistry*, 1996, **271**, 17593-17596.
21. M. Ikeda-Saito, Y. Dou, T. Yonetani, J. S. Olson, T. Li, R. Regan and Q. H. Gibson, *Journal of Biological Chemistry*, 1993, **268**, 6855-6857.
22. D. S. Bohle and C.-H. Hung, *Journal of the American Chemical Society*, 1995, **117**, 9584-9585.
23. S. Amanullah, P. Saha, R. Saha and A. Dey, *Inorganic Chemistry*, 2019, **58**, 152-164.

View Article Online
DOI: 10.1039/D0SC01625J

24. O. Einsle, P. Stach, A. Messerschmidt, J. Simon, A. Kröger, R. Huber and P. M. H. Kroneck, *Journal of Biological Chemistry*, 2000, **275**, 39608-39616.
25. D. Nurizzo, M.-C. Silvestrini, M. Mathieu, F. Cutruzzolà, D. Bourgeois, V. Fülöp, J. Hajdu, M. Brunori, M. Tegoni and C. Cambillau, *Structure*, 1997, **5**, 1157-1171.
26. M. G. Almeida, C. M. Silveira, B. Guigliarelli, P. Bertrand, J. J. G. Moura, I. Moura and C. Léger, *FEBS Letters*, 2007, **581**, 284-288.
27. D. Bykov and F. Neese, *JBIC Journal of Biological Inorganic Chemistry*, 2011, **16**, 417-430.
28. S. E. J. Bowman and K. L. Bren, *Nat Prod Rep*, 2008, **25**, 1118-1130.
29. C. K. Chang and W. Wu, *Journal of Biological Chemistry*, 1986, **261**, 8593-8596.
30. A. M. Stolzenberg, S. H. Strauss and R. H. Holm, *Journal of the American Chemical Society*, 1981, **103**, 4763-4778.
31. S. Ozawa, E. Sakamoto, Y. Watanabe and I. Morishima, *Journal of the Chemical Society, Chemical Communications*, 1994, DOI: 10.1039/C39940000935, 935-936.
32. Y. Liu and M. D. Ryan, *Inorganica Chimica Acta*, 1994, **225**, 57-66.
33. Y. Liu, C. DeSilva and M. D. Ryan, *Inorganica Chimica Acta*, 1997, **258**, 247-255.
34. C. K. Chang, K. M. Barkigia, L. K. Hanson and J. Fajer, *Journal of the American Chemical Society*, 1986, **108**, 1352-1354.
35. S. Ozawa, E. Sakamoto, T. Ichikawa, Y. Watanabe and I. Morishima, *Inorganic Chemistry*, 1995, **34**, 6362-6370.
36. D. W. Feng, Y. S. Ting and M. D. Ryan, *Inorganic Chemistry*, 1985, **24**, 612-617.
37. E. Fujita and J. Fajer, *Journal of the American Chemical Society*, 1983, **105**, 6743-6745.
38. D. Lancon and K. M. Kadish, *Journal of the American Chemical Society*, 1983, **105**, 5610-5617.
39. C. K. Chang and J. Fajer, *Journal of the American Chemical Society*, 1980, **102**, 848-851.
40. M. H. Barley and T. J. Meyer, *Journal of the American Chemical Society*, 1986, **108**, 5876-5885.
41. M. H. Rahman and M. D. Ryan, *Inorganic Chemistry*, 2017, **56**, 3302-3309.
42. Y. Liu and M. D. Ryan, *Journal of Electroanalytical Chemistry*, 1994, **368**, 209-219.
43. I. K. Choi, Y. Liu, D. Feng, K. J. Paeng and M. D. Ryan, *Inorganic Chemistry*, 1991, **30**, 1832-1839.
44. M. R. Kumar, D. Pervitsky, L. Chen, T. Poulos, S. Kundu, M. S. Hargrove, E. J. Rivera, A. Diaz, J. L. Colón and P. J. Farmer, *Biochemistry*, 2009, **48**, 5018-5025.
45. R. Lin and P. J. Farmer, *Journal of the American Chemical Society*, 2000, **122**, 2393-2394.
46. L. E. Goodrich, S. Roy, E. E. Alp, J. Zhao, M. Y. Hu and N. Lehnert, *Inorganic Chemistry*, 2013, **52**, 7766-7780.
47. C. K. Chang, *Biochemistry*, 1980, **19**, 1971-1976.
48. C.-B. Wang and C. K. Chang, *Synthesis*, 1979, **1979**, 548-549.
49. S. Amanullah, P. K. Das, S. Samanta and A. Dey, *Chemical Communications*, 2015, **51**, 10010-10013.
50. J. K. Laha, S. Dhanalekshmi, M. Taniguchi, A. Ambroise and J. S. Lindsey, *Organic Process Research & Development*, 2003, **7**, 799-812.
51. L. W. Olson, D. Schaeper, D. Lancon and K. M. Kadish, *Journal of the American Chemical Society*, 1982, **104**, 2042-2044.
52. L. A. Bottomley and K. M. Kadish, *Inorganic Chemistry*, 1981, **20**, 1348-1357.
53. M. D. Bartberger, W. Liu, E. Ford, K. M. Miranda, C. Switzer, J. M. Fukuto, P. J. Farmer, D. A. Wink and K. N. Houk, *Proceedings of the National Academy of Sciences*, 2002, **99**, 10958.
54. J. Pellegrino, S. E. Bari, D. E. Bikiel and F. Doctorovich, *Journal of the American Chemical Society*, 2010, **132**, 989-995.
55. L. E. Goodrich, F. Paulat, V. K. K. Praneeth and N. Lehnert, *Inorganic Chemistry*, 2010, **49**, 6293-6316.
56. A. P. Hunt and N. Lehnert, *Accounts of Chemical Research*, 2015, **48**, 2117-2125.
57. K. M. Vogel, P. M. Kozlowski, M. Z. Zgierski and T. G. Spiro, *Journal of the American Chemical Society*, 1999, **121**, 9915-9921.
58. C. M. Coyle, K. M. Vogel, T. S. Rush, P. M. Kozlowski, R. Williams, T. G. Spiro, Y. Dou, M. Ikeda-Saito, J. S. Olson and M. Z. Zgierski, *Biochemistry*, 2003, **42**, 10342-10342.
59. S. Rinaldo, A. Arcovito, M. Brunori and F. Cutruzzolà, *Journal of Biological Chemistry*, 2007, **282**, 14761-14767.
60. A. L. Speelman and N. Lehnert, *Accounts of Chemical Research*, 2014, **47**, 1106-1116.
61. Z. Wei and M. D. Ryan, *Inorganic Chemistry*, 2010, **49**, 6948-6954.
62. A. E. Servid, A. L. McKay, C. A. Davis, E. M. Garton, A. Manole, P. S. Dobbin, M. A. Hough and C. R. Andrew, *Biochemistry*, 2015, **54**, 3320-3327.
63. J. J. Warren, T. A. Tronic and J. M. Mayer, *Chemical Reviews*, 2010, **110**, 6961-7001.
64. D. D. M. Wayner and V. D. Parker, *Accounts of Chemical Research*, 1993, **26**, 287-294.
65. V. Shafirovich and S. V. Lymar, *Proceedings of the National Academy of Sciences*, 2002, **99**, 7340.
66. M. A. Rhine, A. V. Rodrigues, R. J. B. Urbauer, J. L. Urbauer, T. L. Stemmler and T. C. Harrop, *Journal of the American Chemical Society*, 2014, **136**, 12560-12563.
67. M. Ali, N. Stein, Y. Mao, S. Shahid, M. Schmidt, B. Bennett and A. A. Pacheco, *Journal of the American Chemical Society*, 2019, **141**, 13358-13371.
68. M. C. Silvestrini, M. G. Tordi, G. Musci and M. Brunori, *Journal of Biological Chemistry*, 1990, **265**, 11783-11787.
69. T. Vangberg and A. Ghosh, *Journal of the American Chemical Society*, 1999, **121**, 12154-12160.
70. W. R. Scheidt, H. F. Duval, T. J. Neal and M. K. Ellison, *Journal of the American Chemical Society*, 2000, **122**, 4651-4659.
71. E. G. Abucayon, R. L. Khade, D. R. Powell, Y. Zhang and G. B. Richter-Addo, *Journal of the American Chemical Society*, 2016, **138**, 104-107.
72. E. G. Abucayon, R. L. Khade, D. R. Powell, M. J. Shaw, Y. Zhang and G. B. Richter-Addo, *Dalton Transactions*, 2016, **45**, 18259-18266.
73. N. G. Connelly, P. T. Draggett, M. Green and T. A. Kuc, *Journal of the Chemical Society, Dalton Transactions*, 1977, DOI: 10.1039/DT9770000070, 70-73.
74. T. C. Harrop, Z. J. Tonzetich, E. Reisner and S. J. Lippard, *Journal of the American Chemical Society*, 2008, **130**, 15602-15610.
75. M. J. T. e. a. Frisch, *Gaussian, Inc.*, 2004, **version C.02**.

View Article Online
DOI: 10.1039/D0SC01625J

76. R. Krishnan, J. S. Binkley, R. Seeger and J. A. Pople, *The Journal of Chemical Physics*, 1980, **72**, 650-654.
77. A. D. McLean and G. S. Chandler, *The Journal of Chemical Physics*, 1980, **72**, 5639-5648.
78. M. Cossi, N. Rega, G. Scalmani and V. Barone, *Journal of Computational Chemistry*, 2003, **24**, 669-681.
79. B. J. Littler, M. A. Miller, C.-H. Hung, R. W. Wagner, D. F. O'Shea, P. D. Boyle and J. S. Lindsey, *The Journal of Organic Chemistry*, 1999, **64**, 1391-1396.

TOC